

1 **Bedload transport measurements with impact plate geophones in two** 2 **Austrian mountain streams (Fischbach and Ruetz): system** 3 **calibration, grain size estimation, and environmental signal pick-up**

4 Dieter Rickenmann¹, Bruno Fritschi¹

5 ¹Swiss Federal Research Institute WSL, Birmensdorf, 8903, Switzerland

6 *Correspondence to:* Dieter Rickenmann (dieter.rickenmann@wsl.ch)

7 **Abstract.**

8 The Swiss plate geophone system is a bedload surrogate measuring technique that has been installed in more than 20
9 streams, primarily in the European Alps. Here we report about calibration measurements performed in two mountain streams
10 in Austria. The Fischbach and Ruetz gravel–bed streams are characterized by important runoff and bedload transport during
11 the snowmelt season. A total of 31 (Fischbach) and 21 (Ruetz) direct bedload samples were obtained during a six year
12 period. Using the number of geophone impulses and total transported bedload mass for each measurement to derive a
13 calibration function, results in a strong linear relation for the Fischbach, whereas there is only a poor linear calibration
14 relation for the Ruetz measurements. Instead, using geophone impulse rates and bedload transport rates indicates that two
15 power law relations best represent the Fischbach data, depending on transport intensity; for lower transport intensities, the
16 same power law relation is also in reasonable agreement with the Ruetz data. These results are compared with data and
17 findings from other field sites and flume studies. We further show that the observed coarsening of the grain size distribution
18 with increasing bedload flux can be qualitatively reproduced from the geophone signal, when using the impulse counts along
19 with amplitude information. Finally, we discuss implausible geophone impulse counts that were recorded during periods
20 with smaller discharges without any bedload transport, and that are likely caused by vehicle movement very near to the
21 measuring sites.

22 **1 Introduction**

23 In the past decade or so, an increasing number of studies were undertaken on bedload surrogate acoustic measuring
24 techniques which were tested both in flume experiments and in field settings. A review of such indirect bedload transport
25 measuring techniques was recently published by Rickenmann (2017a, 2017b). Examples of measuring systems include the
26 Japanese pipe microphone (Mizuyama et al., 2010a, 2010b; Uchida et al. 2013; Goto et al. 2014), the Swiss plate geophone
27 (Rickenmann and Fritschi, 2010, Rickenmann et al. 2012, 2014), other impact plate systems (Krein et al., 2008, 2016; Møen
28 et al. 2010; Reid et al. 2007; Beylich and Laute 2014; Taskiris et al. 2014), and hydrophones, i.e. underwater microphones
29 (Barton et al. 2010; Camenen et al. 2012; Rigby et al. 2015). It is well known that bedload transport rates often show very

30 large variability for given flow conditions (Gomez, 1991; Leopold and Emmett, 1997; Ryan and Dixon, 2008; Recking,
31 2010), and that prediction of (mean) bedload transport rates is still very challenging, particularly for steep and coarse-
32 bedded streams (Bathurst et al., 1987; Nitsche et al., 2011; Schneider et al. 2015, 2016). For such conditions, direct bedload
33 transport measurements are typically difficult to obtain, or may be impossible to make during high flow conditions (Gray et
34 al., 2010). In contrast, indirect bedload transport measuring methods have the advantage of providing continuous monitoring
35 data both in time and over a cross-sections, even during difficult flow conditions, and are therefore expected to increase our
36 understanding of bedload transport.

37 A fair number of these measuring techniques have been successfully calibrated for total bedload flux, which generally
38 requires contemporaneous direct bedload transport measurements in the field (Thorne, 1985, 1986; Voulgaris et al., 1995;
39 Rickenmann and McArdell, 2007, 2008; Mizuyama et al. 2010b; Rickenmann et al. 2014; Mao et al., 2016; Habersack et al.
40 2016; Kreisler et al. 2016). Essentially, linear or power law relations were established between a simple metric
41 characterizing the acoustic signal and bedload mass. In some studies further calibration relations were established to identify
42 particle size, either based on signal amplitude (Mao et al., 2016; Wyss et al., 2016a) and/or on characteristic frequency of
43 that part of the signal which is associated with a single impact of a particle (e.g. for impact plate systems; Wyss et al., 2016b)
44 or by determining a characteristic frequency for an entire grain size mixture (for the hydrophone system; Barrière et al.,
45 2015a). A few of the acoustic measuring techniques were used to determine bedload transport by grain size classes (Mao et
46 al., 2016; Wyss et al., 2016a). Finally, some studies examined to what extent findings from flume experiments can be
47 quantitatively transferred and applied to field sites for which independent, direct calibration measurements exist (Mao et al.,
48 2016; Wyss et al., 2016b, 2016c).

49 In this study we report on calibration measurements of the Swiss plate geophone (SPG) system in two mountain streams
50 in Austria. The Fischbach and Ruetz gravel-bed streams are characterized by important runoff and bedload transport during
51 the snowmelt season. During a six year period, 31 (Fischbach) and 21 (Ruetz) direct bedload samples were obtained in the
52 two streams, respectively. The objectives of this paper are: (i) to present and discuss different ways of analysing the
53 geophone calibration measurements, also in comparison with data and findings from other field sites and flume studies; (ii)
54 to show that the observed coarsening of the grain size distribution with increasing bedload flux can be qualitatively
55 reproduced from the geophone signal; and (iii) to discuss implausible geophone impulse counts that were recorded during
56 periods with small discharge and without any bedload transport, and that are probably associated with close-by vehicle
57 movement.

58 **2 Field sites and calibration measurements**

59 **2.1 Overview of field sites and geophone measurements**

60 The first indirect bedload transport measurements using impact plates were made in the Erlenbach from 1986 to 1999 using a
61 piezoelectric crystal as sensor, with the aim of continuously monitoring the intensity of bedload transport and its relation to

62 stream discharge (Bänziger and Burch, 1990; Rickenmann, 1994, 1997; Hegg et al., 2006; Rickenmann and McARDell,
63 2007). A geophone sensor was used at the Erlenbach and at all other field sites that were set up in the year 2000 and later
64 (Rickenmann and Fritschi, 2010). In the meantime, the SPG system has been installed in more than 20 streams primarily in
65 Central Europe (Rickenmann, 2017b). An array of steel plates is typically installed flush with the surface of a sill or check
66 dam, a location where there is only a small chance for (substantial) deposition of bedload grains during transport conditions.

67 The Fischbach and Ruetz field sites were installed by the Tyrolean Hydropower Company (TIWAG). They are located in
68 partly glaciated catchments in the Tyrolean Alps (Fig. 1), at elevations of 1544 m a.s.l. (Fischbach) and 1688 m a.s.l.
69 (Ruetz). Thus, the streams have a nival and glacial runoff regime, with typical daily discharge variations and regular bedload
70 transport during snow and glacier melt in spring and summer. At both field sites, water discharge and bedload transport have
71 been monitored since 2008. The stream cross-section is essentially trapezoidal at both measuring sites, with the banks
72 protected by riprap and inclined at 45° (Fig. 2, 3). The geophone sensors are fixed in a cylindrical aluminium case and are
73 mounted on the underside and in the middle of stainless steel plates, which are screwed into supporting steel constructions
74 (UPN profiles) and are acoustically isolated by elastomer elements. The steel plates are 0.360 m long, 0.496 m wide, and
75 0.015 m thick. The entire steel construction is 8.2 m long (transvers to the flow direction) and embedded into a concrete sill,
76 founded two meters into the river bed. The entire concrete structure is 8.7 m wide, and it is laterally inclined at 5% to the
77 river left side (Fig. 3), which improves the discharge measurements at low flows. The steel plates are horizontal in flow
78 direction (no longitudinal slope). The sill is protected with riprap on the up- and downstream side. Starting with the first steel
79 plate located 0.35 m from the right bank, every second steel plate is equipped with a geophone sensor, so that there are a
80 total of eight sensors at each site. The riprap on the downstream side of the sill is inclined at about 15% over a length of
81 about 2 m.

82 At both sites, the concrete sill is located 4 m downstream of the cross-section where flow stage is measured on the left
83 side of the stream, and where flow velocity measurements are made by TIWAG to establish a flow rating curve. At the
84 Fischbach, a bridge crosses the stream some 13 m upstream of the concrete sill, and provides vehicle access to the measuring
85 hut on the left side on a small forest road with very infrequent traffic. Along the right side of the stream a local paved road
86 passes nearby, situated only in 5 m horizontal and about 4.5 m vertical distance above the concrete sill with the geophone
87 plates (Fig. 3). Uphill the road leads to the village of Gries with about 200 inhabitants. This is the only village to be accessed
88 upstream of the measuring site. In winter it serves as a relatively small ski resort. At the Ruetz, a bridge crosses the stream
89 some 15 m upstream of the concrete sill, and provides vehicle access to a large parking lot, paved with gravel, on both sides
90 of the stream. The measuring site is located at Mutterbergalm in the Stubai valley. From there a cable car provides access to
91 a large skiing area (winter) and to a hiking area (summer) in the mountains. The public road ends at Mutterbergalm. The
92 parking lot is situated in a similar minimal distance to the measuring cross section as at the Fischbach, i.e. with about 5 m
93 horizontal and 4.5 m to 5 m vertical distance above the concrete sill. This information is important for the analysis and
94 interpretation of the pick-up of geophone signal by environmental sources other than bedload transport.

95 **2.2 Direct bedload measurements for system calibration**

96 At each of the two sites, a streamlined metal pillar was installed 0.5 m downstream of the plate with the geophone sensor no.
97 5 to facilitate the calibration measurements. The metal pillar has a height of 2.5 m and a maximum width of 0.25 m and
98 ensures that a pressure–difference type metal basket sampler fits snugly onto the bed and can be held in place during the
99 bedload sampling operation (Fig. 2b). The aperture of the basket is 50 cm by 50 cm, the same width as the sensor plate. The
100 basket has a notch (cut–out) at a downstream distance of 0.45 m from the aperture (Fig. S1, Supporting information). The
101 notch is somewhat larger than the cross–section of the metal pillar, and the inside of the notch is equipped with rollers. This
102 system allows an exact positioning of the basket during geophone calibration measurements. The maximum width of the
103 basket is 0.90 m and the total length is 2.10 m. During operation the upper surface of the sampler is horizontal while the
104 lower surface is declined at 15% in the downstream direction, in line with the artificial bed in the vicinity of the metal pillar.
105 Over the 0.80 m tail–end of the sampler, the top and sidewall surfaces of the basket are made of 10 mm metal wire mesh.
106 The total volume of the basket is about 0.91 m³.

107 The calibration measurements used here were obtained by TIWAG in both streams during the summer months of 2008 –
108 2013 using the basket bedload sampler. A total of 31 measurements from the Fischbach and 21 measurements from the
109 Ruetz were used in this analysis (Table 1). The maximum sample mass caught in the sampler was 518 kg (including particles
110 finer than 10 mm) in the Fischbach; assuming a bulk density of 1600 kg m⁻³, the bedload volume of this sample was about
111 0.32 m³ or about a third of the total sampler volume. Four calibration measurements from the Fischbach could not be used
112 due to overfilling of the sampler. The grain size distribution of the samples was determined by sieve analysis by a TIWAG–
113 owned engineering consultant. A line–by–number analysis was performed in both streams in October 2012 to estimate the
114 grain size distribution of the bed surface upstream of the geophone sites (Fig. 4).

115 **2.3 Signal pre–processing, recorded geophone values, and amplitude histogram analysis**

116 The bedload impact shocks on the steel plate are transmitted to the geophone sensor and, thereby, an electrical potential is
117 produced. The standard geophone sensor uses a magnet in a coil as an inductive element. The magnet picks up the vibrations
118 of the steel plate and induces a current in the coil which is proportional to the velocity of the magnet. Whenever the voltage
119 exceeds a preselected threshold amplitude value, A_{\min} , the shock is recorded as an impulse, *IMP*. Contrary to all the other
120 sites equipped with an SPG system, the threshold amplitude value A_{\min} used to determine *IMP* values was set at 0.07 V at the
121 Fischbach and Ruetz (Tables 2, 3). The reason is that the first regular geophone recordings in the Fischbach had shown
122 maximum amplitudes in excess of 10 V, the upper limit of the recording system. To increase the resolution of large
123 amplitudes, the raw signal was dampened by about 30%. To compensate for lower signal strength in relation to the impulse
124 counts, the threshold amplitude value A_{\min} was also reduced by 30% when compared with a typical value of 0.1 V used at
125 other sites.

126 At most of the field sites with SPG measurements, several signal summary values were routinely stored in the past. The
 127 most often used summary value for calibration purposes are the summed impulse counts *IMP*. These values were found to
 128 correlate reasonably well with bedload mass or volume transported (Rickenmann and McArdell, 2007, 2008; Rickenmann et
 129 al., 2012, 2014). Another useful summary value is maximum amplitude *MaxA* that may be determined for different recording
 130 intervals. During calibration measurements, all summary values were typically stored in 1 second intervals. During normal
 131 flow monitoring, the recording interval for the summary values at the Fischbach and Ruetz was 15 minutes. (At other SPG
 132 measurement sites operated by WSL this recording interval is typically 1 minute).

133 Using the so-called amplitude histograms (AH), Wyss et al. (2016, 2014) demonstrated for the SPG measurements at the
 134 Erlenbach (Swiss Prealps) that absolute bedload masses for each grain size class could be successfully calculated for both the
 135 calibration and validation data obtained with the moving basket samplers. The continuous recording of AH data was also
 136 implemented at the Fischbach and Ruetz measuring sites, with a recording interval of 1 minute. At these sites, impulses were
 137 determined separately for 17 amplitude classes as listed in Table 2. For the analysis in this study, for each amplitude
 138 threshold value A_{th} (upper class boundary value) a corresponding particle size D was estimated according to an empirical
 139 relation given in Wyss et al. (2016c, Eq. 11) and reported in Appendix A as Eq. (A1).

140 3. Results

141 3.1 Calibration relations for bedload mass and bedload flux using impulse counts

142 The following calibration relations and calibration coefficients were determined using the transported bedload mass M , for
 143 particles with D larger than 10 mm, the impulses *IMP* summed over the sampling period of duration T_s :

$$144 \quad M = k_{lin} IMP \quad (1)$$

$$145 \quad M = k_{pow} IMP^e \quad (2)$$

$$146 \quad k_{tot} = \Sigma M / \Sigma IMP \quad (3)$$

147 where the units are in [kg] for M and for the coefficients (k_{lin} , k_{pow} , k_{tot}), and the Σ sign implies a summation over all the
 148 calibration measurements per site. Equations (1) and (2) were obtained from a linear regression (using log values in case of
 149 Eq. 2), while Eq. (3) represents a mean, linear calibration coefficient based on the total mass and the total number of
 150 impulses for all calibration measurements taken together. The resulting coefficients (k_{lin} , k_{pow} , k_{tot}), exponents (e) and
 151 statistical properties of the calibration relations are reported in Table 3. The squared correlation coefficient r^2 was
 152 determined between the measured masses M and the estimated masses M_{reg} (using eq. 1, 2, or k_{tot} in eq. 2). The relative
 153 standard deviation $s_{e,r}$ is determined for the ratios (M_{reg}/M), using the regression relation to determine M_{reg} from the recorded
 154 impulses *IMP*.

155 For the Fischbach, the calibration relations in the form of Eqs. (1) and (2) show a rather high correlation coefficient (Fig.
 156 5, Table 3), which is also characteristic for similar calibration relations determined for the Erlenbach (Rickenmann et al.,
 157 2012, 2014). For the Ruetz, the calibration relations in the form of Eqs. (1) and (2) are less well defined (Fig. 6, Table 3).
 158 Due to the inclusion of four additional calibration measurements obtained in 2012 and 2013, the correlation coefficient for
 159 the Ruetz is lower than in an earlier analysis that used only 17 measurements from the period 2008 to 2011 (Rickenmann et
 160 al., 2014). This level of correlation is similar to calibration measurements obtained for the Navisence stream in Switzerland
 161 (Wyss et al., 2016c) for which most measured bedload masses were smaller than 20 kg; for the Ruetz, 15 out of 21
 162 calibration measurements also have bedload masses smaller than 20 kg. Using the k_{tot} coefficient from Eq. (3) in Eq. (1)
 163 results in very similar statistical properties as compared to using k_{in} in Eq. (1); while the relative standard deviation $s_{e,r}$
 164 very similar for the Fischbach in both cases, it is about 25% larger for the Ruetz when using the k_{tot} coefficient as compared
 165 to using the k_{in} coefficient (Table 3).

166 Systematic flume experiments were performed for different grain size classes to investigate the dependence of a linear
 167 calibration coefficient, defined as $k_{\text{bj}} = \text{IMP}/M$, on grain size D (Wyss et al., 2016b). This study used bedload particles from
 168 four streams including the Ruetz and Fischbach, and it was found that k_{bj} values showed a local maximum at a grain size D
 169 of around 40 mm, in agreement with earlier flume experiments using quartz spheres of different diameters (Rickenmann et
 170 al., 2014). Therefore, we analysed the field calibration measurements from the Ruetz and Fischbach in a similar way (Fig. 7),
 171 and these data essentially confirmed the findings from the flume experiments. The bedload samples from the Ruetz and
 172 Fischbach show a general tendency for D_{84} to increase with increasing unit bedload transport rate q_b (Fig. 8), where D_{84} is
 173 the grain size for which 84 % of material by weight are finer (determined for particles with $D > 10$ mm). It is therefore not
 174 surprising that k_{bj} values also exhibit a local maximum when plotted against the impulse rate, IMPT (Fig. 9), which is a
 175 proxy for transport rate, and where $\text{IMPT} = \text{IMP}/(T_s w_p)$, with the plate width $w_p = 0.5$ m. Finally this lead us to determine
 176 alternative calibrations in terms of unit bedload transport rate per plate width $q_{b,p}$ as a function of impulse rate, IMPT (Fig.
 177 10), with a limiting value of around 0.5 to 1 ($0.5^{-1} \text{ m}^{-1} \text{ s}^{-1}$) to separate the two ranges with a different power law function:

$$178 \quad q_{b,p} = a_1 \text{IMPT}^{b_1} \quad \text{for } \text{IMPT} < 0.48 \text{ (} 0.5^{-1} \text{ m}^{-1} \text{ s}^{-1} \text{)} \quad (4)$$

$$179 \quad q_{b,p} = a_2 \text{IMPT}^{b_2} \quad \text{for } \text{IMPT} > 0.48 \text{ (} 0.5^{-1} \text{ m}^{-1} \text{ s}^{-1} \text{)} \quad (5)$$

180 where the units for $q_{b,p}$ are in ($\text{kg } 0.5^{-1} \text{ m}^{-1} \text{ s}^{-1}$) and for IMPT in ($0.5^{-1} \text{ m}^{-1} \text{ s}^{-1}$), and the coefficients and exponents are given in
 181 Table 3. Here, we determined $q_{b,p}$ and IMPT deliberately per unit width of one plate since using the traditional 1 m unit
 182 width would result in different coefficients a_1 and a_2 (and a different threshold value IMPT separating the application range
 183 of Eq. 4 and Eq. 5), which would entail the risk of erroneous transformations of measured IMPT values into $q_{b,p}$ values for
 184 each plate.

185 In Fig. 10, the regression relation for higher impulse rates was derived based on 14 calibration measurements from the
 186 Fischbach with $\text{IMPT} > 1$ [$(1/0.5) \text{ m}^{-1} \text{ s}^{-1}$]. Similarly, the regression relation for lower impulse rates was derived based on 17
 187 measurements from the Fischbach and 19 measurements from the Ruetz, all with $\text{IMPT} < 1$ [$(1/0.5) \text{ m}^{-1} \text{ s}^{-1}$]. The two power

188 law relations intersect at $IMPT = 0.48 [(1/0.5) \text{ m}^{-1} \text{ s}^{-1}]$. Using this limiting value, they were applied to the Fischbach and
189 Ruetz data, resulting in the statistical properties of the calibration relations (4) and (5) as reported in Table 3. It appears that
190 the data from both channel sites can be described reasonably well with these calibrations relations, the relative standard
191 deviation $s_{e,r}$ being about 98% for the higher impulse rates and about 110% for the higher impulse rates (Table 3). If Eqs.
192 (4) and (5) are applied to all calibration measurements of each stream separately, the clearly better statistical properties result
193 for the Fischbach ($r^2 = 0.97$, $s_{e,r} = 61 \%$) than for the Ruetz ($r^2 = 0.50$, $s_{e,r} = 145 \%$). In comparison to the calibration relation
194 determined with Eq. (2) for the Fischbach, Eqs. (4) and (5) will predict larger bedload transport rates for very small or very
195 large $IMPT$ values (Fig. 10).

196 **3.2 Coarsening of grain sizes with increasing bedload flux reflected in geophone signal**

197 The amplitude histograms (AH data) for each calibration measurement were used to estimate grain size distributions (GSD)
198 for the basket sampler measurements, which were then compared with the sieve analyses of the bedload samples. For the
199 analysis of the AH data, the lowest class with impulses for $A_{\max} < 0.056 \text{ V}$ was excluded, as this class represents
200 predominantly signal noise. For the remaining 16 classes the sum of the impulses per amplitude class was determined for all
201 1 min time steps for the duration T_s . This resulted in the proportion of impulses per amplitude class per calibration
202 measurement, not yet weighted for grain size. The impulses per class were weighted by the geometric mean diameter of each
203 class (Table 2) to the 2nd power, D_m^2 , to estimate the cumulative distribution of AH-values; this weighting procedure
204 corresponds essentially to the method of Wyss et al. (2016), which is summarized in Appendix A. It is also noted that the
205 start (and end) time of the bedload sampling does not exactly correspond to the start (and end) time of the recorded AH data,
206 which introduced a further (generally minor) uncertainty when interpolating AH data for the first and last recording time step
207 of each bedload sampling period. For the results shown in Figures 10 and 11, the GSD was averaged for given classes of unit
208 bedload transport rates q_b , assigning the same weight to each measurement in a given q_b class. Bedload transport classes and
209 corresponding abbreviation names are defined in Fig. 11 and 12.

210 For the bedload samples from both Fischbach and Ruetz a general coarsening trend of the grain size distribution (GSD)
211 with increasing unit bedload transport rate q_b can be observed, in agreement with general bedload transport theory (Parker,
212 2008). However, GSDs from individual calibration measurements are quite variable within given classes of q_b , both for the
213 bedload samples and for the estimated GSD from the AH values, and do not necessarily follow the general trend. The GSDs
214 estimated from the AH values generally show a qualitatively similar trend as the GSDs from the direct bedload samples, but
215 with a limited quantitative agreement between the two methods.

216 For the Fischbach (Fig. 11) it is noted that only 2 calibration samples were available for the class Fi1, and these had the 2
217 smallest bedload masses (with 19 and 8 kg, respectively); this may be a reason for the poor agreement between estimated
218 and measured GSDs. Similarly, the largest q_b class Fi4 for the Fischbach includes only 1 bedload sample. For the Ruetz (Fig.
219 12) we note that for the classes Ru1 and Ru3 the bedload masses were relatively small, including only 5 to 6 kg. Together
220 with a small number of bedload samples (3 and 2, respectively), this may again be one reason for the relatively poor

221 agreement between estimated and measured GSDs. In contrast, the bedload masses for the Ruetz for the class Ru2 (11 to 23
222 kg) and Ru4 (15 to 129 kg) were clearly larger.

223 3.3 Environmental noise pick-up of the geophone signal

224 Both measuring stations are situated at a relatively high elevation, and the stream catchments include mountain peaks with
225 elevations above 3000 m a.s.l. Therefore the runoff during the winter period is very low, with a base flow below $0.6 \text{ m}^3 \text{ s}^{-1}$ at
226 the Fischbach and below $0.3 \text{ m}^3 \text{ s}^{-1}$ at the Ruetz. During such flow conditions, only about half or two thirds of the sill with
227 the steel plates is submerged under water (Fig. 2, Fig. S2). However, during winter geophone impulses are regularly
228 recorded at all the geophone sensors in both streams (Fig. 13, Fig. 14). According to hydraulic calculations and observations
229 the sill becomes fully submerged for flows of about $2.5 \text{ m}^3 \text{ s}^{-1}$ at the Fischbach and about $2.0 \text{ m}^3 \text{ s}^{-1}$ at the Ruetz. Therefore it
230 is unlikely that these geophone impulses are the result of bedload transport.

231 For the Fischbach and the discharge classes smaller than $3 \text{ m}^3 \text{ s}^{-1}$ the mean *IMP* values per 15 minutes (*IMP*₁₅) vary
232 between about 0.3 and 2.0. A similar analysis as in Fig. 13 but with a finer discharge resolution (classes of $0.25 \text{ m}^3 \text{ s}^{-1}$) is
233 presented in Fig. S3. It is also obvious that plates (sensors) no. 1 to 3 generally recorded more impulses than the other plates
234 no. 4 to 8 (Fig. 13, Fig. S3), which is unlikely a result of bedload transport. For discharges up to about $3 \text{ m}^3 \text{ s}^{-1}$ traffic noise
235 appears to be a likely source of the geophone impulses, since the local road passes on the river right side very close to the
236 plates no. 1 to 3 (Fig. 2). For discharge classes larger than $4 \text{ m}^3 \text{ s}^{-1}$ the plates no. 4 to 8 (which have a larger water depth than
237 plates no. 1 to 3) start to record more impulses on average (*IMP*₁₅) than plates no. 1 to 3; in addition the *IMP*₁₅ values start to
238 increase with increasing discharge (Fig. 13, Fig. S3). This behaviour is more in line with expectations from bedload–
239 transport induced signals.

240 For the Ruetz and the discharge classes smaller than $1.0 \text{ m}^3 \text{ s}^{-1}$ the mean *IMP*₁₅ values vary between about 0.2 and 2.0.
241 Plates no. 5 to 8 generally recorded more impulses than the other plates no. 1 to 4 (Fig. 14, Fig. S4). The plates no. 1 to 3 are
242 typically not submerged during these flow conditions, and no signal is to be expected from bedload transport. Again, traffic
243 noise appears to be a likely source of the measured geophone impulses. The plates on the river left side (5 to 8) tend to
244 register more impulses on average because the access road to the parking lot passes on this side, hence more parking traffic
245 is to be expected. A clearer dominance of the plates no. 5 to 8 (which have a larger water depth than plates no. 1 to 4)
246 becomes apparent for discharge classes larger than about $1.5 \text{ m}^3 \text{ s}^{-1}$ at the Ruetz (Fig. 14, Fig. S4), which is in line with
247 expectations from bedload–transport induced signals. The mean value of *IMP*₁₅ averaged over all eight plates becomes larger
248 than about 2 for discharges larger than roughly $2.0 \text{ m}^3 \text{ s}^{-1}$, and above this discharge level the *IMP*₁₅ values start to increase in
249 general with increasing discharge.

250 To further investigate the potential source of the implausible geophone recordings, we classified the measured *IMP*₁₅
251 values into 15 minute intervals during each day–time (Figs. S5, S6). For both streams and low flows, there is a clear daily
252 cycle of geophone impulse activity although discharge remains rather constant during the entire day. This pattern clearly is
253 present for the Fischbach for discharges *Q* smaller than about $3 \text{ m}^3 \text{ s}^{-1}$ and for the Ruetz for *Q* smaller than about $1.5 \text{ m}^3 \text{ s}^{-1}$.

254 Geophone activity is higher during the afternoon and the first half of the night at the Fischbach, and primarily during day
255 time at the Ruetz. A clear absence of this or a similar daily pattern is evident for the Fischbach for Q larger than about $6 \text{ m}^3 \text{ s}^{-1}$
256 1 and for the Ruetz for Q larger than about $3.5 \text{ m}^3 \text{ s}^{-1}$ (Fig. S5, S6). This is a further indication that the geophone impulses at
257 smaller discharges are mainly traffic induced. Taken together, the above analysis and interpretation suggests that bedload
258 transport may be the dominant source of producing geophone impulses above a critical discharge Q_c of about $3.5 \text{ m}^3 \text{ s}^{-1}$ at the
259 Fischbach, and above a Q_c of about $1.5 \text{ m}^3 \text{ s}^{-1}$ at the Ruetz.

260 Turowski et al. (2011) analysed the start and end of bedload transport in gravel-bed streams, including geophone
261 measurements from the Fischbach and Ruetz for the years 2008 and 2009. They determined discharge values at the start (Q_s)
262 and at the end (Q_e) of a transport period for the Fischbach and the Ruetz streams. The Q_s and the Q_e values that are smaller
263 than the Q_c values identified in this study for the two streams, respectively, may contain implausible impulse counts. It is
264 estimated that Turowski et al. (2011) used about 62 % (out of 95 measurements) potentially implausible values for the
265 Fischbach and about 41 % (out of 492 measurements) potentially implausible values for the Ruetz. If these values were
266 discarded from their analysis, this would change the histograms of the discharge at the start and end of transport for the two
267 streams but it would not affect the general conclusions of the study of Turowski et al. (2011).

268 4. Discussion

269 4.1 Calibration relations for the Swiss plate geophone system and grain size determination

270 For a system such as the Swiss plate geophone it is known that the signal response depends on factors such as grain size,
271 fluid or particle velocity, particle shape and mode of transport (i.e. sliding, rolling, saltating), and impact angle and impact
272 location on the steel plate (e.g. Wyss et al., 2016b; Rickenmann, 2017b). For a given stream we may assume that the most of
273 these factors vary within a given range, and the linear calibration coefficients primarily vary with flow conditions. Therefore,
274 we expect that the mean signal response from a given particle size traveling over the plate becomes more stable the larger is
275 the total number of particles that have been transported over the plate. This is the main reason why we have primarily
276 considered the summed geophone summary values in the past (e.g. Rickenmann et al., 2012, 2014). Calibration
277 measurements from various sites confirmed the expectation that random factors influencing the signal response tend to be
278 more averaged out for longer integration periods (Rickenmann and McArdell, 2007, 2008; Rickenmann et al., 2012, 2014;
279 Wyss et al., 2016a, 2016c).

280 However, it may also be interesting to consider calibration relations for example between bedload rates and impulse
281 rates. If a linear calibration relation in the form of Eq. (1) is generally valid, a division of M and IMP by the sampling
282 duration T_s to determine rates will typically result in similar values for the linear calibration coefficient. Having performed
283 this alternative analysis in terms of bedload rates and impulse rates for the data of this study, two distinctly different ranges
284 of geophone signal response were found based on the data from the Fischbach (Fig. 10). These calibration measurements
285 suggest that two power law calibration relations in terms of rates provide a better fit than a single linear calibration relation

286 for the entire domain. The existence of two different ranges is likely a result of a changing GSD with increasing bedload
287 transport rates. We therefore also plotted data from calibration measurements at many other sites (Fig. 15), but no clear trend
288 for a similar pattern can be observed for most of these sites. The only exception is the Urslau stream in Austria; the
289 individual calibration measurements for this stream indicate a trend for a power law relation between q_b and $IMPT$ with an
290 exponent $b < 1$ for smaller q_b values and with an exponent $b > 1$ for larger q_b values (Kreislner et al., 2016). These calibration
291 measurements cover a range of about three orders of magnitude of q_b values; however different methods were used to obtain
292 the bedload samples for smaller and larger bedload transport intensities, and for the smaller range of q_b values the number of
293 measurements is limited.

294 For extreme flow conditions and very high bedload transport rates, there may be some limitations to extrapolating
295 calibration relations for the SPG system from the typical range of conditions investigated so far. Using the same steel impact
296 plates, we had installed piezoelectric bedload impact sensors (PBIS) in an earlier study to make bedload measurements at a
297 water intake of the Pitzbach mountain stream in Austria during two summer periods (Rickenmann and McArdell, 2008).
298 Impulses were counted in a similar way as for the Swiss plate geophone system. At the Tyrolean weir a total of 12 steel
299 plates with sensors were installed, with a natural gravel-bed surface upstream of the sill of 6 m width. Pressure sensors in the
300 settling basin downstream of the Tyrolean weir provided direct measurements of bedload volumes for calibration.
301 Downstream of the settling basin there is a flushing canal, where 3 steel plates with sensors were installed at the end of a 1.5
302 m wide concrete channel. Flushing of sediment from the settling basin occurred over relatively short time periods and thus
303 produced high velocity flows and much higher bedload concentrations in the flow than at the (natural) approach flow to the
304 Tyrolean weir. While a reasonably well defined calibration relation could be obtained for the measurements at the Tyrolean
305 weir (Rickenmann and McArdell, 2008), a very large scatter was observed for the calibration data of the flushing canal, for
306 bedload volumes smaller than 100 m^3 (Fig. S9). This observation indicates that there are limitations for the SPG system for
307 extreme flow conditions. There is also evidence from debris-flow observations at the Illgraben torrent in Switzerland with a
308 geophone sensor mounted underneath a large steel plate (McArdell et al., 2007) that the calibration relations for the SPG
309 system obtained for bedload transport cannot be directly applied to estimate the mass of debris flows. A somewhat similar
310 limitation was observed for the Japanese pipe microphone system, for which signal “saturation” may occur for high bedload
311 transport rates, probably because this system is more sensitive to particle sizes smaller than 10 mm as compared to the SPG
312 system (Wyss et al, 2016a; Rickenmann, 2017a, 2017b).

313 We used the AH data recorded during the calibration measurements at the Fischbach and Ruetz to estimate the
314 transported bedload mass for each calibration measurement, M_{est} , by applying the procedure presented by Wyss et al.
315 (2016a). This method is summarized in Appendix A, and it was specifically developed for the measuring conditions at the
316 Erlenbach stream in Switzerland. Here, we used Eq. (A3) with the coefficient and exponent determined from the Erlenbach
317 measurements; the relation of Eq. (A3) is expected to vary somewhat from site to site, and its application here is therefore
318 associated with uncertainty. To assess the performance of this procedure when applied to the Fischbach and Ruetz, we
319 plotted the ratio of estimated to observed bedload mass, M_{est}/M , as a function of bedload transport rate per plate $q_{b,p}$ and of

320 observed mass M (Fig. 16). There is generally an over-estimation of bedload mass, up to a factor of about 10. Interestingly,
321 the over-estimation decreases with increasing bedload transport rate (Fig. 16a). This result is in agreement with Fig. 15,
322 which suggests that site-specific differences for calibration relations in terms of bedload transport rates and impulse rates
323 tend to be relatively smaller for higher values of q_b . The degree of over-estimation of bedload mass as well as the scatter
324 around a mean trend line for both streams appears to decrease also with increasing bedload mass for the data of the
325 Fischbach and Ruetz (Fig. 16b), but this trend is somewhat less pronounced. Concerning grain size estimation from bedload
326 surrogate measuring techniques, it may be noted that only a few other acoustic measuring techniques were (partly) successful
327 in determining bedload transport by grain size classes from field measurements (Barrière et al., 2015b, using an impact plate
328 hydrophone system; Mao et al., 2016, using a Japanese impact pipe microphone system).

329 To illustrate the uncertainty associated with using different calibration relations, we determined the yearly bedload (YBL)
330 for 2010, which represents the year with the largest peak discharges and the largest YBL values (Table 4) for the period
331 2008–2013. For both streams, the YBL values are larger when using Eqs. (4) and (5) as compared to using Eq. (1); this is not
332 surprising when comparing the linear with the power law calibration relations in Fig. 10. The power law calibration relations
333 result in a 66 % higher YBL for the Fischbach and in a 85 % higher YBL for the Ruetz, if only plausible IMP values for
334 discharges larger than Q_c are considered; the differences are larger if the entire IMP data set for 2010 is considered,
335 including many implausible values recorded during low flow periods (Table 4). The between-stream comparison shows a
336 much larger YBL for the Fischbach than for the Ruetz, which is due to more frequent peak discharges in the Fischbach
337 exceeding about $10 \text{ m}^3 \text{ s}^{-1}$ during the year 2010 (Fig. S7, S8).

338 **4.2 Environmental noise pick-up of the geophone signal**

339 Hydrophones (underwater microphones) have been used to monitor bedload transport both in riverine and in coastal
340 environments (e.g. Thorne, 1990; Camenen et al. 2012; Basset et al., 2013). The objective of using such a system is to record
341 self-generated noise produced by collisions of moving bedload particles against each other or against the bed. The
342 application of this bedload surrogate measuring system can be impaired by other sources of noise, which may be caused by
343 vessel traffic, marine seismic exploration, or underwater military operations. If the main interest is in the acoustic signal due
344 to bedload transport, discounting for other sources of noise may be challenging and will also depend for example on the
345 spatial distance and the dominant frequencies of the different acoustic sources (Hildebrand, 2009; Etter, 2012; Basset et al.,
346 2013).

347 For the application of impact plates with acoustic sensors installed in a streambed there is very few experience with non-
348 bedload transport related sources of noise that may compromise their usefulness. We have shown in section 3.3 that road
349 traffic is a likely source of environmental noise producing a similarly strong signal at the SPG system as low-intensity
350 bedload transport during periods with moderate discharges. This observation was made for our two study streams Fischbach
351 and Ruetz, where in both cases the stream bed runs very close-by to roads, which are located only about half the stream-
352 width away from the edge of the bed. We have checked the impulse counts recorded for SPG systems installed at mountain

353 streams in Switzerland, particularly for low flow periods during winter time. There were generally very few impulses
354 recorded at these sites, indicating that road traffic is not an important source of noise. At these sites roads with regular traffic
355 are situated clearly farther away from the channel profile than at the two Austrian sites of this study: at the Navisence stream
356 in Zinal (Ancey et al., 2015) about 45 m (or 3 times the stream width), at the Albula River in Tiefencastel (Rickenmann et
357 al., accepted) about 30 m (or twice the stream width) to a road or about 15 m to a parking lot of a single building, and at the
358 Avançon de Nant stream near Pont de Nant about 20 m (or 4 times the stream width). The SPG system at the Erlenbach
359 stream in Switzerland (Rickenmann et al., 2012) is situated about 45 m away from a road; at this site we observed
360 implausible impulse counts limited to very short time periods that were likely due to hikers or possibly game passing at the
361 site.

362 At the Riedbach stream in Switzerland the geophone measuring site is situated at a water intake at an elevation of 1800 m
363 a.s.l, with few direct sunshine and often freezing temperatures during winter time. The access road ends at the water intake
364 and is not open to the public. For a seven year period from 2009 to 2015 geophone measurements showed no systematic
365 relationship between *IMP* and *Q* for discharges *Q* smaller than about $0.4 \text{ m}^3 \text{ s}^{-1}$, but a considerable number of *IMP* were
366 recorded for *Q* values as small as $0.05 \text{ m}^3 \text{ s}^{-1}$ (Schneider et al., 2016). These discharge conditions are typical for the winter
367 period, and it was hypothesized that ice transport or break-up may be mainly responsible for the impulse counts. Impulses
368 may be typically as high as between 1 and 100 impulses for all seven plates and for 10 minute recording intervals.
369 Calculating a mean impulse value per plate for $Q < 0.3 \text{ m}^3 \text{ s}^{-1}$ and including also zero values, this results in an average
370 duration of about 5 hours for one impulse to be registered at the Riedbach by one of the seven steel plates. This relatively
371 low occurrence frequency does not contradict the ice transport or break-up hypothesis.

372 **5. Conclusions**

373 The Fischbach and Ruetz gravel-bed streams are characterized by important runoff and bedload transport during the
374 snowmelt season. As a bedload surrogate measuring technique, the Swiss plate geophone (SPG) system has been installed in
375 2007 in both streams. During the six year period 2008 – 2013, 31(Fischbach) and 21 (Ruetz) direct bedload samples were
376 obtained in the two streams, and these measurements were analysed to obtain calibration relations for the SPG system at the
377 two sites.

378 As applied at many other SPG sites in the past, we first established calibration relations using total transported bedload
379 mass and the number of geophone impulses. A second way of analysing the geophone calibration measurements consisted in
380 using bedload transport rates and geophone impulse rates. For the Fischbach the second approach resulted in two power law
381 calibration relations, with different coefficients and exponents for small and large transport rates. The exponent was smaller
382 than one for small transport rates, and larger than one for larger transport rates. For the Ruetz data with essentially only
383 lower transport intensities, the power law relation derived from the Fischbach is also in reasonable agreement with the Ruetz
384 calibration measurements. The non-linear power law calibration relations are in qualitative agreement with the observed

385 coarsening of the bedload with increasing transport rates. According to findings from flume studies the signal response per
386 unit bedload mass increases for small grains up to grain size of approximately 40 mm, and decreases again for larger grains
387 with increasing particle size (Wyss et al., 2016b); this provides qualitative support for the existence of the two power law
388 relations. A similar behaviour could be observed only for the calibration measurements at the Urslau stream in Austria
389 (Kreisler et al., 2016). In contrast, calibration measurements from six other sites, including the Ruetz stream, do not show
390 evidence for the existence of similar two-range power law calibration relations.

391 Amplitude information from the geophone signal was recorded in minute intervals at the Fischbach and Ruetz by
392 summing impulse counts separately for different amplitude classes (so-called AH data). Since signal amplitude correlates
393 with grain size at several SPG sites (Wyss et al., 2016a, 2016b, 2016c), this information was used to estimate the grain size
394 distribution for the bedload samples from the Fischbach and Ruetz. It was found that the observed coarsening of the grain
395 size distribution with increasing bedload flux could be qualitatively reproduced from the geophone signal using the AH data.

396 For smaller discharges at the Fischbach and Ruetz, in particular during the winter time, it was found that many
397 implausible geophone impulse counts were recorded. Both SPG measuring sites are situated very close to local roads with
398 regular traffic. The roads are only about half the stream width away from the steel plates, and we therefore identified vehicle
399 traffic as a likely source for the implausible geophone impulses. This is indirectly supported by a comparison with other SPG
400 sites in Switzerland. At most of these sites only very few implausible geophone impulse counts were recorded in the past,
401 which is probably due to the fact that the local roads are farther away from the steel plates, generally at least once or twice
402 the stream width.

403 **6. Data availability**

404 The data cannot be made publicly available for the time being since it is used by the Tyrolean Hydropower Company
405 TIWAG, the owner and provider of the data, in an ongoing hydropower project authorisation procedure.

406 **7. Appendix A: Summary of the amplitude histogram method of Wyss et al. (2016a)**

407 Information about the grain-size distribution of the transported bedload over a Swiss geophone plate can be determined
408 using the number of impulses per amplitude class (called amplitude histogram method). Amplitude histograms (AH data)
409 can be interpreted as a statistical distribution of the signal's amplitude over a given time interval. Using the number of
410 bedload particles per unit mass, absolute bedload masses for each grain-size class were calculated for the Erlenbach stream
411 in Switzerland.

412 For j grain size classes an amplitude threshold value A_{th} (upper class boundary value, in V) corresponds to a threshold
413 particle size D in (mm) separating the grain size class (Wyss et al. 2016a). In this study an empirical relation given in Wyss
414 et al. (2016c) was used (see also Table 2):

415 $D = 85.5 A_{th}^{0.41}$ (A1)

416 Wyss et al. (2016a) assumed that the number of impulses per amplitude class, IMP_j , are related to the number of particles in
 417 the corresponding grain size class, N_j , with a mean weight, G_{mj} , by a coefficient α_j determined from the bedload samples, as
 418 follows:

419 $IMP_j = \alpha_j N_j$ (A2)

420 For the calibration of the method for the Erlenbach 31 bedload samples were used. The analysis resulted in the following
 421 empirical power law relation between α_j and the class mean grain size D_{mj} in [mm] where the median value of α_j of all
 422 bedload samples was used to determine the empirical relation (A3):

423 $\alpha_j = 0.0093 D_{mj}^{1.09}$ (A3)

424 where the coefficient 0.0093 has the units [$\text{mm}^{-1.09}$]. Finally, to estimate the bedload mass per grain size class, the following
 425 relation can be used:

426 $M_{est} = N_j G_{mj} = \frac{IMP_j G_{mj}}{\alpha_j}$ (A4)

427 The above procedure was used to estimate the bedload mass for each calibration sample from the Fischbach and the Ruetz,
 428 as reported in section 4.1 in the Discussion. To determine the mean weight, G_{mj} in [g] for each grain size class with D_{mj} in
 429 [mm], the following empirical relations were used, based on investigations reported in Wyss et al. (2016c):

430 $G_{mj} = 0.00165 D_{mj}^{2.94}$ for the Fischbach (A5)

431 $G_{mj} = 0.00111 D_{mj}^{3.03}$ for the Ruetz (A6)

432 Considering Eqs. (A5) or (A6) together with Eqs. (A3) and (A4) it follows that the mass of grains per class is approximately
 433 proportional to $IMP_j \bullet D_{mj}^2$. We used this proportionality in section 3.2 to estimate the GSD for the calibration measurements
 434 from the Fischbach and Ruetz based on the recorded AH data. The main uncertainty in transferring the method of Wyss et al.
 435 (2016a) determined for the Erlenbach to another site is the use of Eq. (A3) which may be different at other sites. We used the
 436 entire procedure reported here, including Eq.(A3) with the coefficient and exponent determined from the Erlenbach
 437 measurements, in section 4.1 to explicitly estimate the total bedload mass for each calibration measurement from the
 438 Fischbach and Ruetz based on the recorded AH data.

439 **8. Supplement link**

440 → see also Supplementary Material

441 **9. Author contribution**

442 BF was the main responsible for the concept and installation of the SPG system at the Fischbach and Ruetz. He had
443 suggested to record the AH data as a memory efficient way to extract grain-size relevant information from the raw geophone
444 signal. DR was responsible for the analysis and wrote the paper. Support of colleagues for figure preparation is
445 acknowledged below.

446

447 **10. Acknowledgements**

448 We are grateful to the Tyrolean Hydropower Company (TIWAG) for having performed the geophone calibration
449 measurements in the Fischbach and Ruetz streams and for having provided these data and the continuous geophone
450 measurements to WSL for further analysis. The study was supported by SNF grants 200021_124634 and 200021_137681.
451 We thank Nicloas Steeb, Philipp von Arx, and Thomas Weninger for help with the preparation of some figures; TW also
452 performed grain size analyses of the streambed surface. We thank Alexandre Badoux for constructive comments on the
453 manuscript submitted as Discussion paper.

454

455 **11. References**

456

- 457 Ancey, C., Bohorquez, P., and Bardou, E.: Sediment transport in mountain rivers, ERCOFTAC Bulletin, 100, 37–52, 2015.
- 458 Bänziger, R., and Burch, H.: Acoustic sensors as indicators for bed load transport in a mountain torrent, in: Hydrology in
459 Mountainous Regions I, IAHS. Publ. no. 193, pp. 207–214, 1990.
- 460 Barrière, J., Krein, A., Oth, A., and Schenkluhn, R.: An advanced signal processing technique for deriving grain size
461 information of bedload transport from impact plate vibration measurements, Earth Surf. Proc. Land., 40, 913–924, 2015a.
- 462 Barrière, J., Oth, A., Hostache, R., and Krein, A.: Bed load transport monitoring using seismic observations in a low-
463 gradient rural gravel bed stream, Geophys. Res. Lett., 42, 2294–2301, 2015b.
- 464 Barton, J. S., Slingerland, R. L., Pittman, S., and Gabrielson, T. B.: Monitoring coarse bedload transport with passive
465 acoustic instrumentation: A field study, in: U.S. Geological Survey Scientific Investigations Report 2010–5091, 38–51,
466 available at: <https://pubs.usgs.gov/sir/2010/5091/papers/listofpapers.html>, 2010.
- 467 Bassett, C., Thomson, J., and Polagye, B.: Sediment-generated noise and bed stress in a tidal channel, J. Geophys. Res.
468 Oceans, 118, 2249–2265, 2013.
- 469 Bathurst, J. C., Graf, W. H., and Cao, H. H.: Bed load discharge equations for steep mountain rivers, in: Sediment transport
470 in gravel-bed rivers, Wiley & Sons, New York, USA, 453–477, 1987.

471 Beylich, A. A., and Laute, K.: Combining impact sensor field and laboratory flume measurements with other techniques for
472 studying fluvial bedload transport in steep mountain streams, *Geomorphology*, 218, 72–87, 2014.

473 Camenen, B., Jaballah, M., Geay, T., Belleudy, P., Laronne, J. B., and Laskowski, J. P.: Tentative measurements of bedload
474 transport in an energetic alpine gravel bed river, in: *River Flow 2012*, Taylor & Francis Group, London, 379–386, 2012.

475 Gomez, B.: Bedload transport, *Earth–Sci. Rev.*, 31, 89–132, 1991.

476 Goto, K., Itoh, T., Nagayama, T., Kasai, M., and Marutani, T.: Experimental and theoretical tools for estimating bedload
477 transport using a Japanese pipe hydrophone, *Int. J. Erosion Control Engineering*, 7(4), 101–110, 2014.

478 Gray, J. R., Laronne, J. B., and Marr, J. D. G.: Bedload–surrogate Monitoring Technologies, U.S. Geological Survey
479 Scientific Investigations Report 2010–5091, 37p., available at: <http://pubs.usgs.gov/sir/2010/5091/>, 2010.

480 Fehr, R.: A method for sampling very coarse sediments in order to reduce scale effects in movable bed models, in
481 *Proceedings of IAHR Symposium on Scale Effects in Modelling Sediment Transport Phenomena*, 383–397, Toronto,
482 Canada, 1987.

483 Habersack, H., Kreisler, A., Rindler, R., Aigner, J., Seitz, H., Liedermann, M., and Laronne, J. B.: Integrated automatic and
484 continuous bedload transport monitoring in gravel bed rivers, *Geomorphology*, doi:10.1016/j.geomorph.2016.10.020,
485 2016.

486 Hegg, C., McArdell, B. W., and Badoux, A.: One hundred years of mountain hydrology in Switzerland by the WSL, *Hydrol.*
487 *Process.*, 20, 371–376, 2006.

488 Krein, A., Klinck, H., Eiden, M., Symader, W., Bierl, R., Hoffmann, L., and Pfister, L.: Investigating the transport dynamics
489 and the properties of bedload material with a hydro–acoustic measuring system, *Earth Surf. Proc. Land.*, 33, 152–163,
490 2008.

491 Kreisler, A., Moser, M., Aigner, J., Rindler, R., Tritthard, M., and Habersack, H.: Analysis and classification of bedload
492 transport events with variable process characteristics, *Geomorphology*, doi:10.1016/j.geomorph.2016.06.033, 2016.

493 Leopold, L. B., and Emmett, W. W.: Bedload and river hydraulics – Inferences from the East Fork River, Wyoming, U.S.
494 Geological Survey Professional Paper 1583, 1997.

495 Mao, L., Carrillo, R., Escauriaza, C., and Iroume, A.: Flume and field–based calibration of surrogate sensors for monitoring
496 bedload transport, *Geomorphology*, 253, 10–21, 2016.

497 McArdell, B. W., Bartelt, P., and Kowalski, J.: Field observations of basal forces and fluid pore pressure in a debris flow,
498 *Geophys. Res. Lett.*, 34, L07406, doi:10.1029/2006GL029183, 2007.

499 Mizuyama, T., Oda, A., Laronne, J. B., Nonaka, M., and Matsuoka, M.: Laboratory tests of a Japanese pipe geophone for
500 continuous acoustic monitoring of coarse bedload, in: U.S. Geological Survey Scientific Investigations Report 2010–
501 5091, 319–335, available at: <https://pubs.usgs.gov/sir/2010/5091/papers/listofpapers.html>, 2010a.

502 Mizuyama, T., Laronne, J. B., Nonaka, M., Sawada, T., Satofuka, Y., Matsuoka, M. et al.: Calibration of a passive acoustic
503 bedload monitoring system in Japanese mountain rivers, in: U.S. Geological Survey Scientific Investigations Report
504 2010–5091, 296–318, available at: <https://pubs.usgs.gov/sir/2010/5091/papers/listofpapers.html>, 2010b.

505 Møen, K. M., Bogen, J., Zuta, J. F., Ade, P. K., and Esbensen, K. Bedload measurement in rivers using passive acoustic
506 sensors, in: U.S. Geological Survey Scientific Investigations Report 2010–5091, 336–351, available at:
507 <https://pubs.usgs.gov/sir/2010/5091/papers/listofpapers.html>, 2010.

508 Nitsche, M., Rickenmann, D., Turowski, J. M., Badoux, A., and Kirchner, J. W.: Evaluation of bedload transport predictions
509 using flow resistance equations to account for macro-roughness in steep mountain streams, *Water Resour. Res.*, 47,
510 W08513, doi:10.1029/2011WR010645, 2011.

511 Recking, A.: A comparison between flume and field bed load transport data and consequences for surface based bed load
512 transport prediction, *Water Resour. Res.*, 46, W03518, doi:10.1029/2009WR008007, 2010.

513 Recking, A.: An analysis of nonlinearity effects on bed load transport prediction, *J. Geophys. Res. Earth Surf.*, 118, 1264–
514 1281, doi:10.1002/jgrf.20090, 2013.

515 Reid, S. C., Lane, S. N., and Berney, J. M.: The timing and magnitude of coarse sediment transport events within an upland
516 gravel-bed river, *Geomorphology*, 83, 152–182, 2007.

517 Rickenmann, D.: Sediment load and discharge in the Erlenbach Stream, in: *Dynamics and Geomorphology of Mountain*
518 *Rivers*, Lecture Notes in Earth Sciences, 52, 53–66, 1994.

519 Rickenmann, D.: Sediment transport in Swiss torrents, *Earth Surf. Proc. Land.*, 22, 937–951, 1997.

520 Rickenmann, D.: Bedload transport measurements with geophones, hydrophones and underwater microphones (passive
521 acoustic methods), in: *Gravel Bed Rivers and Disasters*, Wiley & Sons, Chichester, UK, 185–208, 2017a.

522 Rickenmann, D.: Bedload transport measurements with geophones and other passive acoustic methods, *J. Hydraul. Eng.–*
523 *ASCE*, 143(6), 03117004-1-14, doi: 10.1061/(ASCE)HY.1943-7900.0001300, 2017b.

524 Rickenmann, D., and McArdell, B. W.: Continuous measurement of sediment transport in the Erlenbach stream using
525 piezoelectric bedload impact sensors, *Earth Surf. Proc. Land.*, 32, 1362–1378, 2007.

526 Rickenmann, D., and McArdell, B. W.: Calibration measurements with piezoelectric bedload impact sensors in the Pitzbach
527 mountain stream, *Geodin. Acta*, 21, 35–52, 2008.

528 Rickenmann, D., and Fritschi, B.: Bedload transport measurements using piezoelectric impact sensors and geophones, in:
529 U.S. Geological Survey Scientific Investigations Report 2010–5091, 407–423, available at:
530 <https://pubs.usgs.gov/sir/2010/5091/papers/listofpapers.html>, 2010.

531 Rickenmann, D., Turowski, J. M., Fritschi, B., Klaiber, A., and Ludwig, A.: Bedload transport measurements at the
532 Erlenbach stream with geophones and automated basket samplers, *Earth Surf. Proc. Land.*, 37, 1000–1011, 2012.

533 Rickenmann, D., Turowski, J. M., Fritschi, B., Wyss, C., Laronne, J. B., Barzilai, R. et al.: Bedload transport measurements
534 with impact plate geophones: comparison of sensor calibration in different gravel-bed streams, *Earth Surf. Proc. Land.*,
535 39, 928–942, 2014.

536 Rickenmann, D., Antoniazza, G., Wyss, C. R., Fritschi, B., and Boss, S.: Bedload transport monitoring with acoustic sensors
537 in the Swiss Albula mountain river, *Proc. IAHS*, 375, 5-10, doi:10.5194/piahs-375-5-2017, 2017.

538 Rigby, J. R., Kuhnle, R. A., Goodwiller, B. T., Nichols, M. H., Carpenter, W. O., Wren, D. G., and Chambers, J. P.:
539 Sediment-generated noise (SGN): Comparison with physical bed load measurements in a small semi-arid watershed,
540 Paper presented at the 2015 SEDHYD Conference, 19–23 April 2015, Reno, Nevada, USA, available at:
541 <http://www.sedhyd.org/2015/>, 2015

542 Ryan, S. E., and Dixon, M. K.: Spatial and temporal variability in stream sediment loads using examples from the Gros
543 Ventre Range, Wyoming, USA, in: Gravel-Bed Rivers VI: From Process Understanding to River Restoration, in:
544 Developments in Earth Surface Processes, 11, 387–407, 2008.

545 Schneider, J. M., Rickenmann, D., Turowski, J. M., Bunte, K., and Kirchner, J. W.: Applicability of bed load transport
546 models for mixed-size sediments in steep streams considering macro-roughness, *Water Resour. Res.*, 51, 5260–5283,
547 doi:10.1002/2014WR016417, 2015.

548 Schneider, J. M., Rickenmann, D., Turowski, J. M., Schmid, B., and Kirchner, J. W.: Bed load transport in a very steep
549 mountain stream (Riedbach, Switzerland): Measurement and prediction, *Water Resour. Res.*, 52,
550 doi:10.1002/2016WR019308, 2016.

551 Thorne, P. D.: The measurement of acoustic noise generated by moving artificial sediments, *J. Acoustic Soc. America*, 78,
552 1013–1023, 1985.

553 Thorne, P. D.: Laboratory and marine measurements on the acoustic detection of sediment transport, *J. Acoustic Soc.*
554 *America*, 80, 899–910, 1986.

555 Thorne, P. D.: Seabed generation of ambient noise, *J. Acoustic Soc. America*, 87, 149–153, 1990.

556 Tsakiris, A. G., Papanicolaou, A. N., and Lauth, T. J.: Signature of bedload particle transport mode in the acoustic signal of a
557 geophone, *J. Hydraul. Res.*, 52(2), 185–204, 2014.

558 Turowski, J. M., Badoux, A., and Rickenmann, D.: Start and end of bedload transport in gravel-bed streams, *Geophys. Res.*
559 *Let.*, 38, L04401, doi:10.1029/2010GL046558, 2011.

560 Uchida, T., Okamoto, A., Hayashi, S., Suzuki, T., Fukumoto, A., Yamashita, A., and Tagata, S.: Hydrophone observations of
561 bedload transport in mountainous rivers of Japan, in: *Advances in River Sediment Research*, Taylor & Francis Group,
562 London, 1749–1796, 2013.

563 Voulgaris, G., Wilkin, M. P., and Collins, M. B.: The in situ passive acoustic measurement of shingle movement under
564 waves and currents: instrument (TOSCA) development and preliminary results, *Cont. Shelf Res.*, 15, 1195–1211, 1995.

565 Wyss, C. R., Rickenmann, D., Fritschi, B., Turowski, J. M., Weitbrecht, V., and Boes, R. M.: Measuring bedload transport
566 rates by grain-size fraction using the Swiss plate geophone signal at the Erlenbach, *J. Hydraul. Eng.–ASCE*, 142(5),
567 04016003, doi: 10.1061/(ASCE)HY.1943-7900.0001090, 2016a.

568 Wyss, C. R., Rickenmann, D., Fritschi, B., Turowski, J. M., Weitbrecht, V., and Boes, R. M.: Laboratory flume experiments
569 with the Swiss plate geophone bedload monitoring system. Part I: Impulse counts and particle size identification, *Water*
570 *Resour. Res.*, 52, 7744–7759, doi:10.1002/2015WR018555, 2016b.

571 Wyss, C. R., Rickenmann, D., Fritschi, B., Turowski, J. M., Weitbrecht, V., Travaglini, E., Bardou, E., and Boes, R. M.:
572 Laboratory flume experiments with the Swiss plate geophone bedload monitoring system. Part II: Application to field
573 sites with direct bedload samples, *Water Resour. Res.*, 52, 7760–7778, doi:10.1002/2016WR019283, 2016c.
574
575

577 **Table 1.** Catchment and channel characteristics at the field sites and range of typical parameters for the conditions during the
 578 geophone calibration measurements. The q_b values refer to bedload with $D > 10$ mm.
 579

| | Fischbach | Ruetz |
|--|-----------|------------|
| <i>Catchment parameters</i> | | |
| Drainage area (km ²) | 71 | 28 |
| Maximum elevation (m) | 3497 | 3474 |
| Site elevation (m) | 1540 | 1684 |
| Mean annual precipitation (mm) | 1670 | 1880 |
| % glacier | 16 | 20 |
| <i>Channel parameters (measuring site)</i> | | |
| Gradient over 60 m upstream of geophone site S (%) | 1.7 | 2.5 |
| Stream bed width (m) | 8.5 | 8.5 |
| Bed surface D_{84} (m) | 0.26 | 0.28 |
| Bed surface D_{50} (m) | 0.09 | 0.10 |
| <i>Parameter range for calibration periods</i> | | |
| Period of calibration measurements used in this study | 2008–2013 | 2008–2013 |
| No. of calibration measurements used in this study (n) | 31 | 21 |
| Max. unit discharge q_{\max} (m ² s ⁻¹) | 1.97 | 0.97 |
| Min. unit discharge q_{\min} (m ² s ⁻¹) | 0.56 | 0.41 |
| Max. mean flow velocity V_{\max} (m/s) | 2.79 | 1.88 |
| Min. mean flow velocity V_{\min} (m/s) | 1.51 | 1.02 |
| Max. unit bedload transport rate, $q_{b,\max}$ (kg s ⁻¹ m ⁻¹) | 7.20 | 0.214 |
| Min. unit bedload transport rate, $q_{b,\min}$ (kg s ⁻¹ m ⁻¹) | 0.0050 | 0.0025 |
| Bedload samples: max. D_{\max} (m) | 0.350 | 0.150 |
| Bedload samples: min. D_{\max} (m) | 0.030 | 0.050 |
| Bedload samples: max. weight ($D > 10$ mm) (kg) | 431 | 128 |
| Bedload samples: mean weight ($D > 10$ mm) (kg) | 70.0 | 20.6 |
| Sampling duration of calibration measurements (s) | 30 – 3600 | 600 – 3600 |
| Recording interval of geophone summary values during normal flow monitoring (s) | 900 | 900 |

582

583 **Table 2.** Threshold values of the signal amplitude A used for the impulse count of the amplitude histograms at the Fischbach
584 and Ruetz. To estimate a corresponding particle size D , an empirical relation from Wyss et al. (2016c) was used.
585 D_{mg} is the geometric mean size of each particle class.
586

| | | | | | | | | | | | | | | | | | |
|----------------------|-------|-------|-------|-------|-------|-------|-------|-------|-------|-------|-------|-------|-------|-------|-------|------|------|
| A_{th} (V) | 0.056 | 0.079 | 0.112 | 0.158 | 0.224 | 0.316 | 0.447 | 0.631 | 0.891 | 1.259 | 1.778 | 2.512 | 3.548 | 5.012 | 7.079 | 10.0 | 12.0 |
| D (mm) | 26.2 | 30.2 | 34.8 | 40.1 | 46.3 | 53.3 | 61.5 | 70.8 | 81.5 | 94.0 | 108 | 125 | 144 | 166 | 191 | 220 | 237 |
| D_{mg} (mm) | | 28.1 | 32.4 | 37.4 | 43.1 | 49.7 | 57.2 | 66.0 | 76.0 | 87.5 | 101 | 116 | 134 | 154 | 178 | 205 | 228 |

587

588

589 **Table 3.** Coefficients, exponents and statistical properties for the calibration relations according to eq. 1, 2, 3, 4, 5. All
590 calibration relations refer to bedload mass with $D > 10$ mm, or unit bedload transport rate $q_{b,p}$ for $D > 10$ mm. In
591 the equations, the units are: M in (kg), $q_{b,p}$ in ($\text{kg } 0.5^{-1} \text{ m}^{-1} \text{ s}^{-1}$) and $IMPT$ in ($0.5^{-1} \text{ m}^{-1} \text{ s}^{-1}$). Here r^2 is the correlation
592 coefficient between values calculated with the regression relation and the recorded bedload masses. Similarly, in
593 all figures, r^2 is determined between the predicted y -value and the observed y -value (in the linear domain). The
594 relative standard deviation $s_{e,r}$ is determined for the ratios (M_{est}/M) of estimated bedload mass M_{est} calculated with
595 the regression relation and the recorded impulses IMP , divided by the recorded bedload mass M . For the first three
596 relations, the number of calibration measurements (n) are given in Table1, for the other two relations they are
597 listed in this table.
598

| | Fischbach | Ruetz | both streams |
|---|-----------|---------|--------------|
| $M = k_{lin} IMP$ | | | |
| k_{lin} | 0.0508 | 0.0436 | |
| r^2 | 0.964 | 0.597 | |
| significance level: probability p | <0.0001 | <0.0001 | |
| $s_{e,r}$ | 0.67 | 1.38 | |
| $M = k_{pow} M^e$ | | | |
| k_{pow} | 0.134 | 1.40 | |
| e | 0.88 | 0.42 | |
| r^2 | 0.967 | 0.576 | |
| significance level: probability p | <0.0001 | <0.0019 | |
| $s_{e,r}$ | 0.78 | 0.92 | |
| $M = k_{tot} IMP$ | | | |
| k_{tot} | 0.0558 | 0.0547 | |
| r^2 | 0.964 | 0.597 | |
| significance level: probability p | <0.0001 | <0.0001 | |
| $s_{e,r}$ | 0.73 | 1.73 | |
| $q_{b,p} = a_1 IMPT^{b_1}$ for $IMPT < 0.48$ ($0.5^{-1} \text{ m}^{-1} \text{ s}^{-1}$) | | | |
| a_1 | 0.0237 | 0.0237 | 0.0237 |
| b_1 | 0.48 | 0.48 | 0.48 |
| n | 15 | 15 | 30 |
| r^2 | 0.559 | 0.790 | 0.524 |
| significance level: probability p | <0.0001 | <0.054 | <0.0001 |
| $s_{e,r}$ | 0.77 | 1.13 | 0.98 |
| $q_{b,p} = a_2 IMPT^{b_2}$ for $IMPT > 0.48$ ($0.5^{-1} \text{ m}^{-1} \text{ s}^{-1}$) | | | |
| a_2 | 0.0436 | 0.0436 | 0.0436 |
| b_2 | 1.29 | 1.29 | 1.29 |
| n | 16 | 6 | 22 |
| r^2 | 0.964 | 0.517 | 0.966 |
| significance level: probability p | <0.0001 | <0.0001 | <0.0001 |
| $s_{e,r}$ | 0.37 | 1.71 | 1.11 |

599

600 **Table 4.** Comparison of yearly bedload (*YBL*, in t) calculated with two different calibration relations, for the year 2010 and
 601 for different ranges of *Q* values. The *YBL* values represent transport over the entire stream width; as only every
 602 second steel plate is equipped with a geophone sensor, the loads inferred from the geophone impulses were
 603 multiplied by a factor of 2 in this table.
 604

| Stream | Year | Q range | Yearly bedload | Yearly bedload | YBL-A / YBL-B |
|-----------|------|---|-------------------------|----------------------|---------------|
| | | | YBL-A (t) Eqs. (4,5) | YBL-B (t) Eq. (1) | |
| Fischbach | 2010 | all Q (including im- plausible IMP values) | 10,800 | 6,430 | 1.68 |
| | | $Q > 3.5 \text{ m}^3 \text{ s}^{-1}$ | 10,600 | 6,410 | 1.66 |
| Ruetz | 2010 | all Q (including im- plausible IMP values) | 1,360 | 621 | 2.19 |
| | | $Q > 1.5 \text{ m}^3 \text{ s}^{-1}$ | 1,110 | 600 | 1.85 |

605

606

607

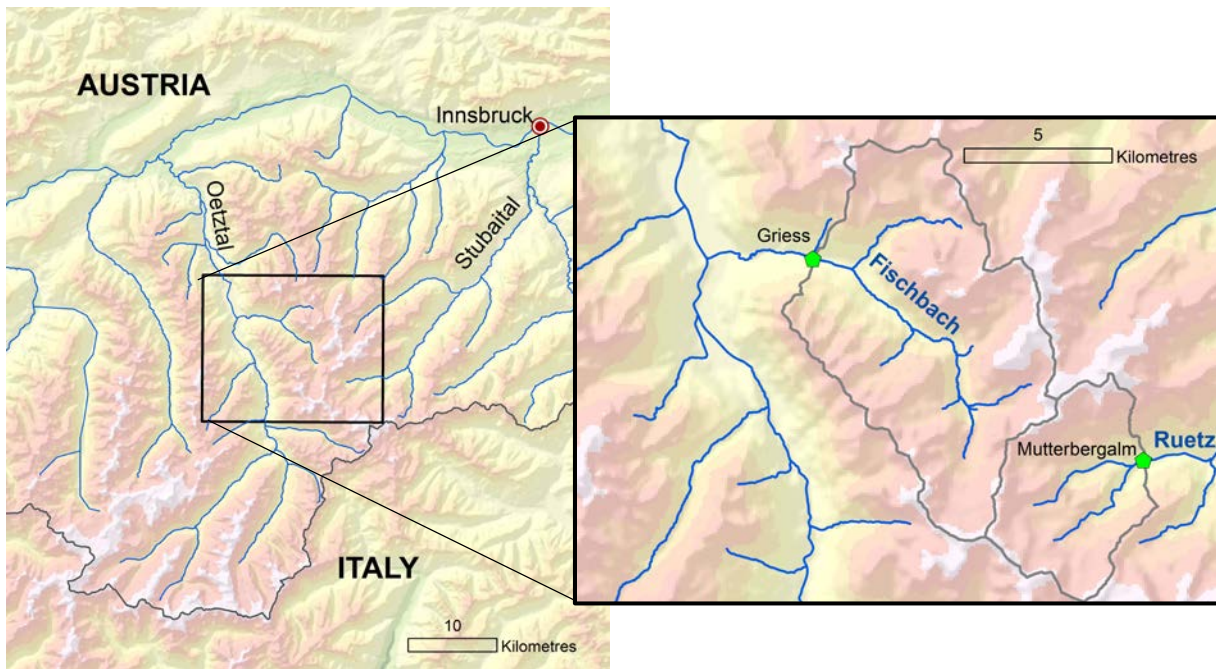


Figure 1. Location of the Fischbach and Ruetz mountain stream catchments in the Stubai Alps of Tyrol in western Austria. The measuring sites are indicated with a green pentagon, and the catchment boundaries are marked with a gray line. (Source of topographic map: Abteilung Geoinformation, Amt der Tiroler Landesregierung; <https://www.tirol.gv.at/data>)

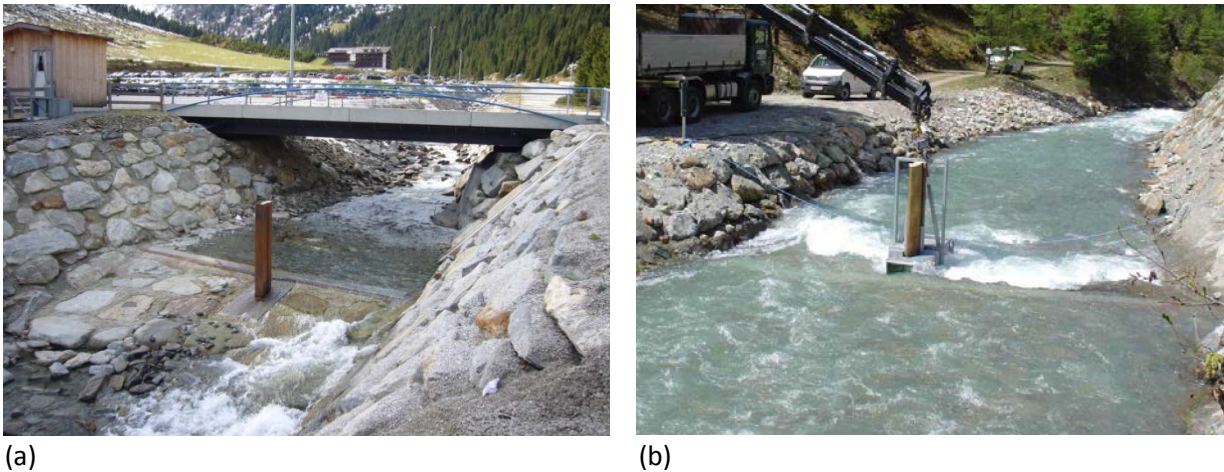


Figure 2. Monitoring sites equipped with a Swiss plate geophone system and a flow gauging station. (a) Ruetz, looking upstream onto the sill with the steel plates (28 October 2009), (b) Fischbach, looking downstream during a calibration measurement using the TIWAG basket sampler (27 May 2008). The steel-concrete pillar visible in both photos is used to guide the positioning of the basket sampler during the collection of bedload samples immediately downstream of the geophone plate.

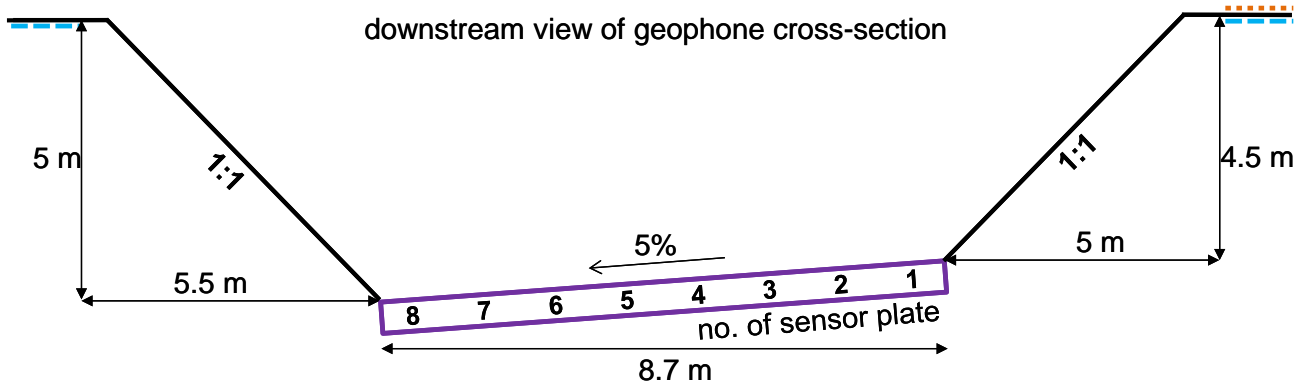


Figure 3. Schematic stream cross-section at the geophone measuring site in both Fischbach and Ruetz. The steel-concrete pillar is located downstream of the sensor plate no. 5. The sill with the steel plates is inclined towards the left bank to improve the resolution of the flow gauge measurements at low discharges. On the banks, the dotted horizontal line indicates the paved local road on river right side at the Fischbach, and the two dashed horizontal lines indicate the graveled parking lot on both river sides at the Ruetz.

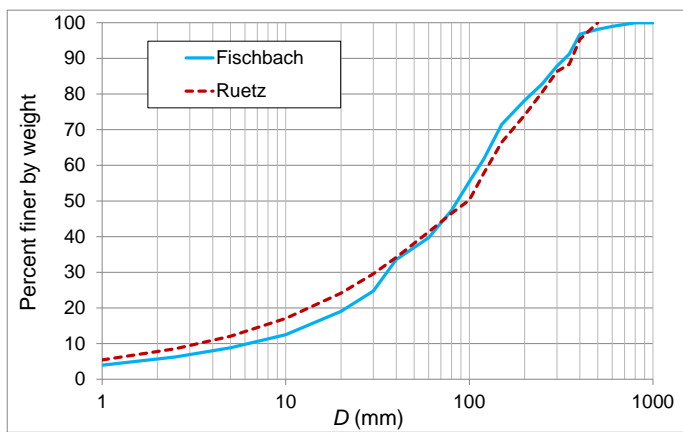


Figure 4. Grain size distribution (GSD) of the surface bed material upstream of the measuring sites. The GSD was measured on 3 October 2012 at the Fischbach and on 4 October 2012 at the Ruetz. The line by number samples included observations for grain sizes $D > 10$ mm, and they were averaged and transformed into a volumetric sample by assuming a 12% unmeasured proportion of $D < 10$ mm (Recking, 2013) and combining it with a Fuller type distribution for the fine material (Fehr, 1987).

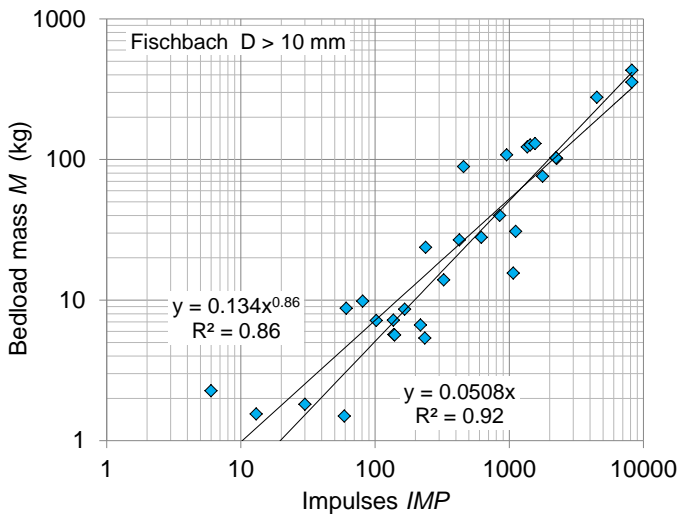


Figure 5. Fischbach: Geophone calibration relationships for grains with $D > 10$ mm between bedload mass M and number of impulses IMP . The linear and power law regression equations are based on 31 calibration measurements for the years 2008-2013.

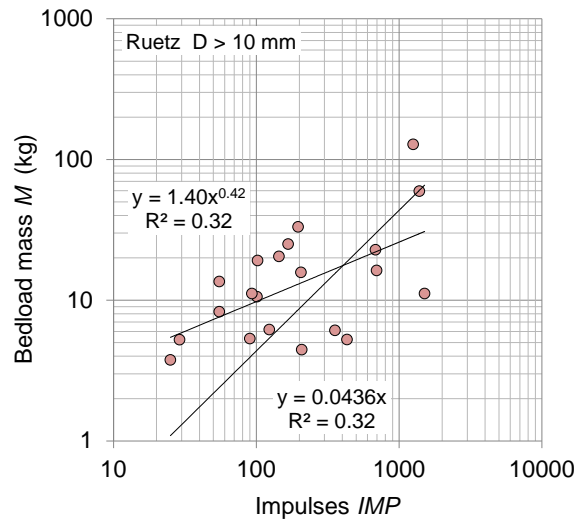


Figure 6. Ruetz: Geophone calibration relationships for grains with $D > 10$ mm between bedload mass M and number of impulses IMP . The linear and power law regression equations are based on 21 calibration measurements for the years 2008-2013.

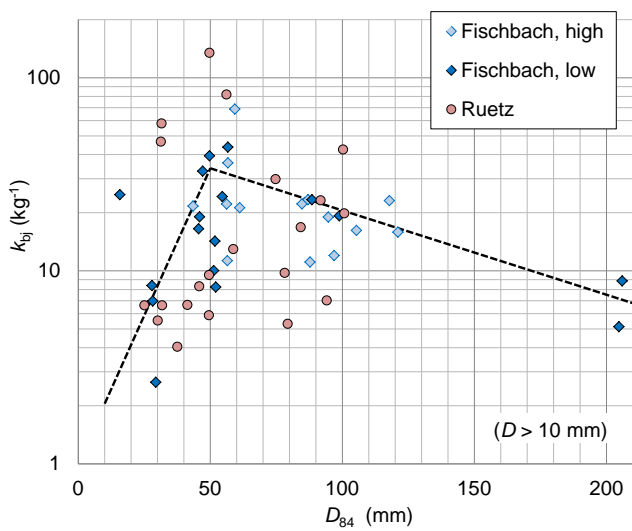


Figure 7. Linear calibration coefficient k_{bj} versus characteristic grain size D_{84} , determined for particles with $D > 10$ mm. Fischbach: data points marked “high” and “low” refer to impulse rates higher and lower than $1 (0.5^{-1} \text{ m}^{-1} \text{ s}^{-1})$, respectively. The dashed lines are meant to guide the eye.

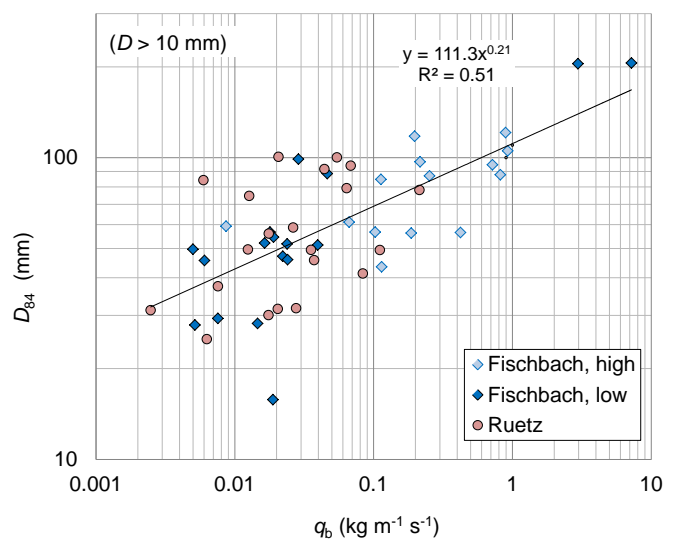


Figure 8. Characteristic grain size D_{84} (determined for particles with $D > 10$ mm) versus bedload flux q_b , derived from the calibration bedload samples (for $D > 10$ mm). Fischbach: data points marked “high” and “low” refer to impulse rates higher and lower than $1 (0.5^{-1} \text{ m}^{-1} \text{ s}^{-1})$, respectively. The regression line is based on both the Fischbach and Ruetz data.

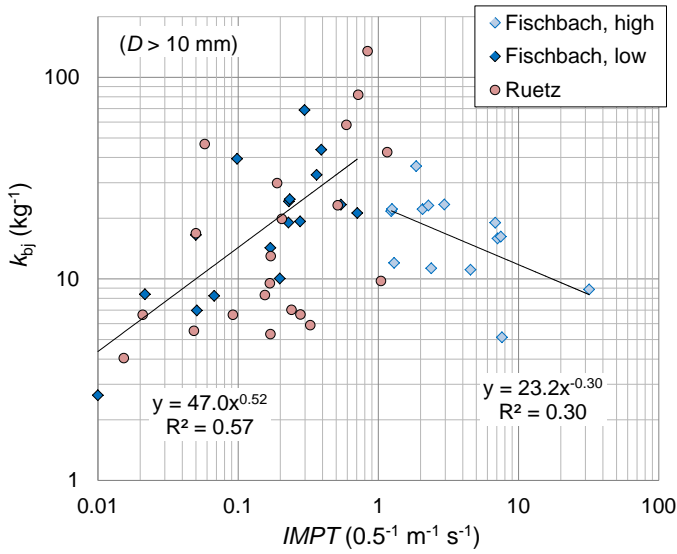


Figure 9. Linear calibration coefficient k_{bj} (for $D > 10 \text{ mm}$) versus impulse rate $IMPT$. Fischbach: data points marked “high” and “low” refer to impulse rates higher and lower than $1 (0.5^{-1} \text{ m}^{-1} \text{ s}^{-1})$, respectively. The regression lines are based on the Fischbach data only.

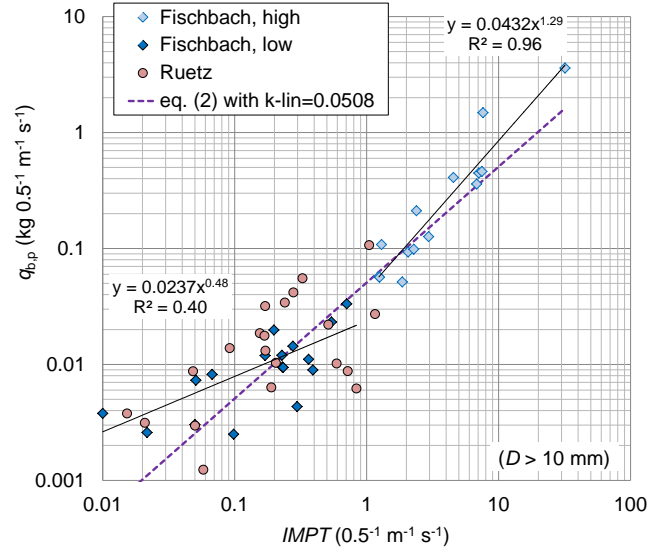
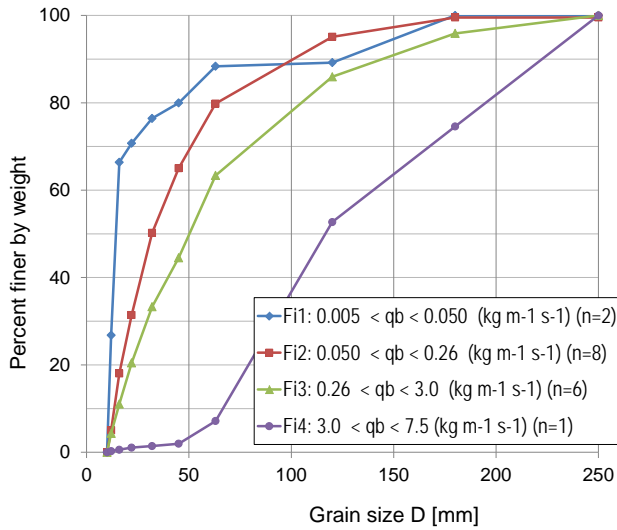
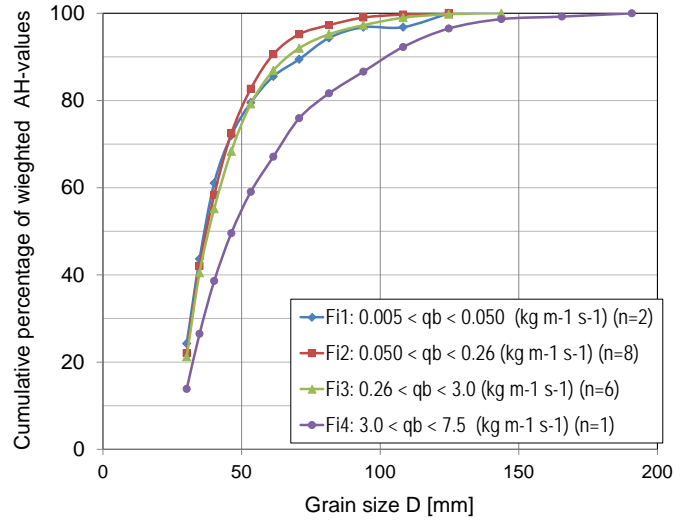


Figure 10. Unit bedload transport rate $q_{b,p}$ for particles $D > 10 \text{ mm}$ vs. impulse rate $IMPT$. Fischbach: data points marked “high” and “low” refer to $IMPT$ values higher and lower than $1 (0.5^{-1} \text{ m}^{-1} \text{ s}^{-1})$, respectively. The regression lines are based on the Fischbach data only. The violet dashed line represents the linear calibration relation Eq. (2) determined for the Fischbach data based on a regression of M vs. IMP .

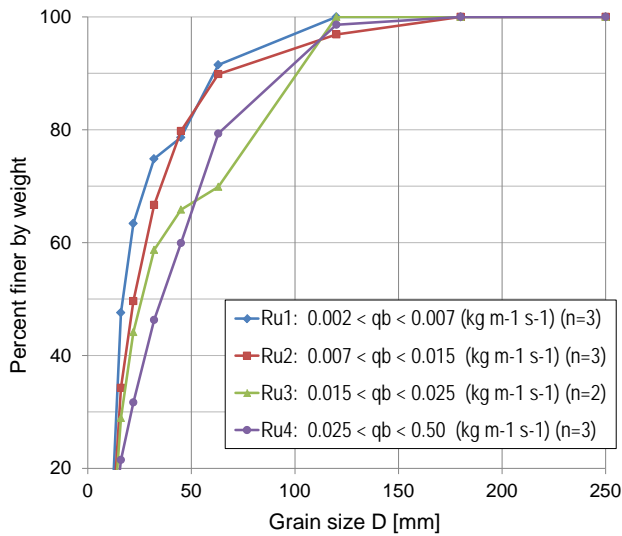


(a)

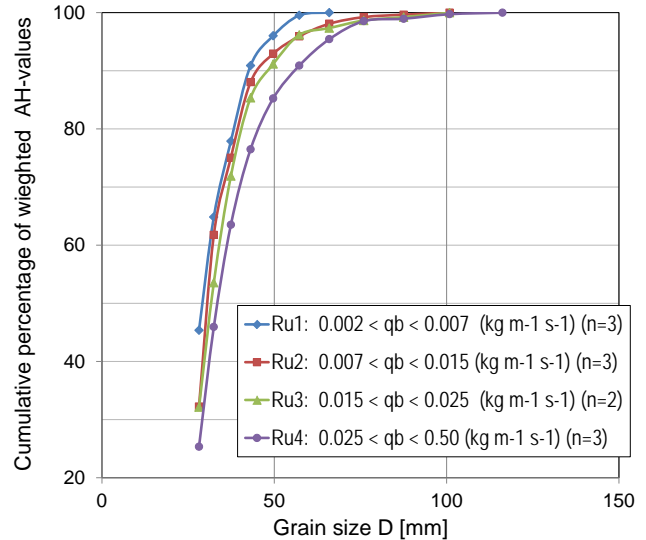


(b)

Figure 11. Fischbach: (a) Grain size distributions derived from the calibration bedload samples (for $D > 10$ mm), averaged for four classes of bedload fluxes q_b (using 17 samples from 2010-2012). (b) Relative distribution of grain sizes estimated from the geophone measurements based on the AH data, averaged for the same four classes of bedload fluxes (using the same 17 sample periods from 2010-2012).



(a)



(b)

Figure 12. Ruetz: (a) Grain size distributions derived from the calibration bedload samples (for $D > 10$ mm), averaged for four classes of bedload fluxes q_b (using 11 samples from 2010-2013). (b) Relative distribution of grain sizes estimated from the geophone measurements based on the AH data, averaged for the same four classes of bedload fluxes (using the same 11 sample periods from 2010-2013).

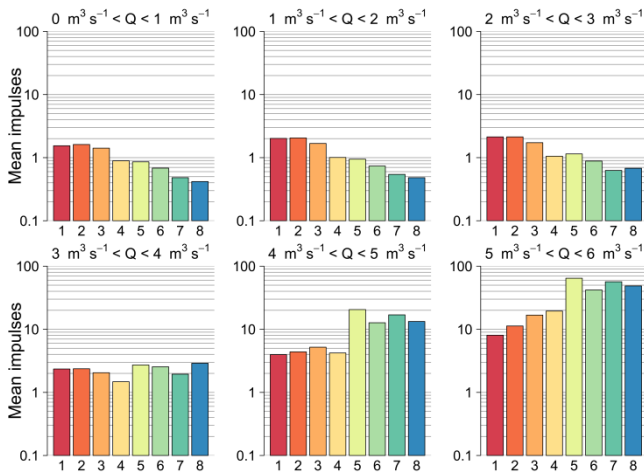


Figure 13. Fischbach: Arithmetic mean of geophone impulses per 15 min for each of the eight plates (ordinates), averaged over the period 2008-2013 and including zero values, for discharge Q classes with width of $1 \text{ m}^3 \text{ s}^{-1}$, for discharges up to $6 \text{ m}^3 \text{ s}^{-1}$.

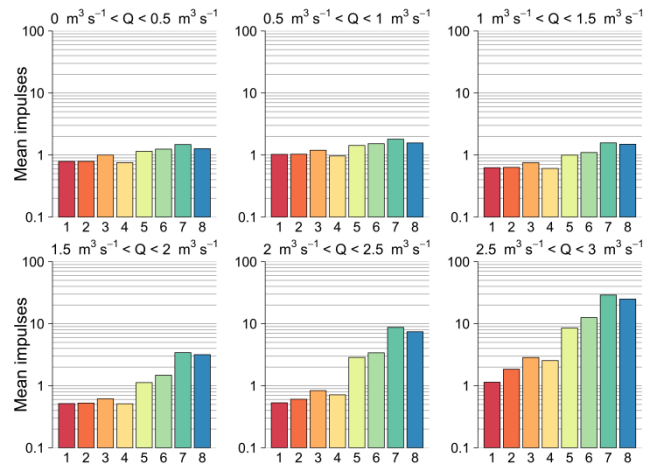


Figure 14. Ruetz: Arithmetic mean of geophone impulses per 15 min for each of the eight plates (ordinates), averaged over the period 2008-2013 and including zero values, for discharge Q classes with width of $0.5 \text{ m}^3 \text{ s}^{-1}$, for discharges up to $3 \text{ m}^3 \text{ s}^{-1}$.

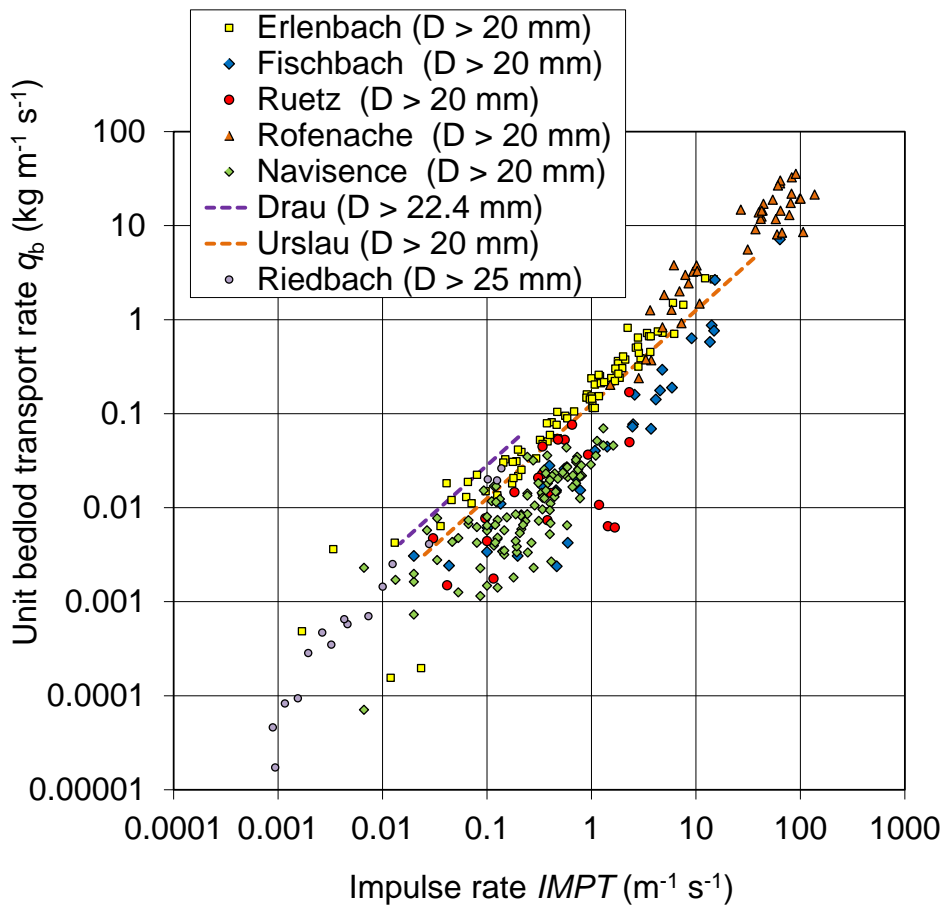


Figure 15. Comparison of geophone calibration data from eight different stream sites. Unit bedload transport rate q_b for particles with D larger than (mostly) 20 mm is plotted against impulse rate $IMPT$. Data sources for additional data are: Wyss et al. (2016c) for Navisence and Erlenbach (some data up to 2016 were added here); Habersack et al. (2016) for Drau; Kreisler et al. (2016) for Urslau (linear calibration relation is approximate; q_b values given for $D > 10 \text{ mm}$ were reduced by factor of 0.68 to estimate q_b values for $D > 20 \text{ mm}$; reduction factor was estimated from 85 samples of Erlenbach moving basket data); Schneider et al. (2016) for Riedbach.

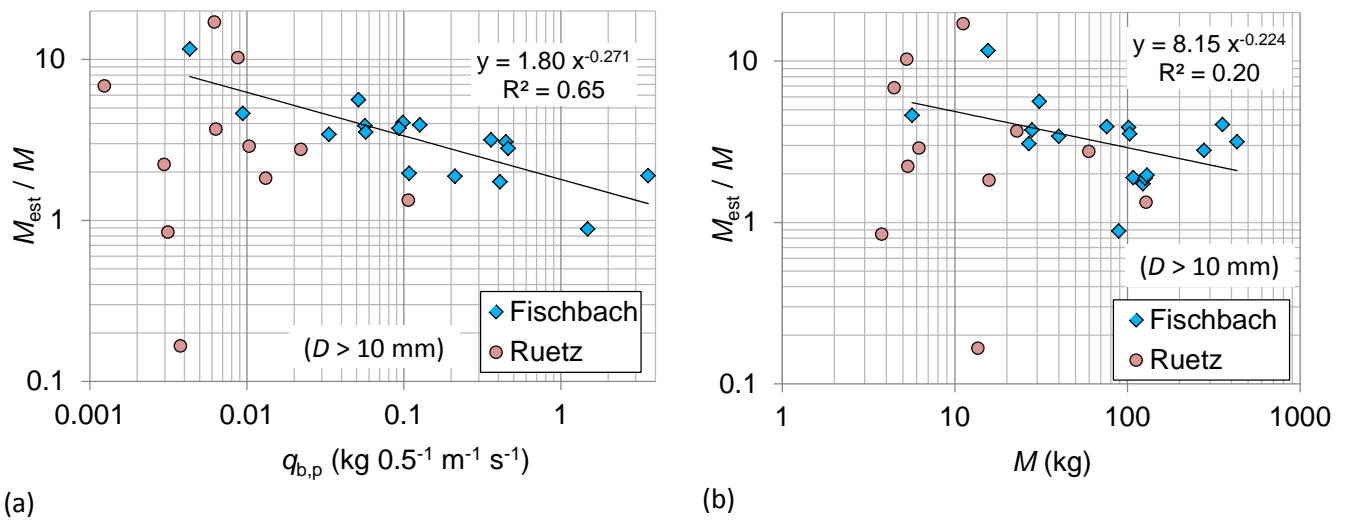


Figure 16. The estimated bedload mass per sample using the method in Wyss et al. (2016a) developed for the Erlenbach, M_{est} , is compared with the measured bedload mass, M , through the ratio M_{est}/M . (a) Ratio M_{est}/M shown vs. unit bedload transport rate $q_{b,p}$ for particles with $D > 10$ mm, (b) Ratio M_{est}/M shown vs. measured bedload Mass M for particles with $D > 10$ mm. In both diagrams the regression line is based on the Fischbach data only.